CrossMark

ORIGINAL PAPER

Influence of process variables on physical characteristics of spray freeze dried cellulose nanocrystals

Wissam Abdallah · Musa R. Kamal (ID)

Abstract This study compares the characteristics of cellulose nanocrystal (CNC) agglomerates prepared using spray drying, freeze drying, and spray freeze drying. Moreover, the effect of the concentration of CNC in the initial aqueous dispersion ($\sim$ 0.5–10.0 wt%) on the morphology, particle size distribution, porosity and crystalline structure of the spray freeze dried CNC agglomerates were investigated. Scanning electron microscopy was used to characterize the morphology and particle size distribution, nitrogen adsorption–desorption isotherms were used to analyze the porous structure of the particles, and X-ray diffraction was used to analyze the crystalline structure of the pa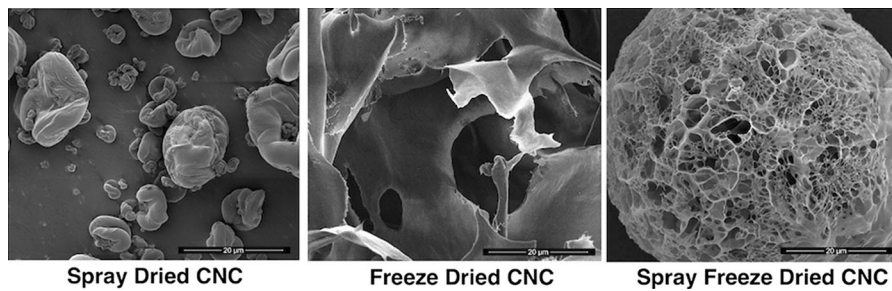rticles. Spray drying of CNC resulted in 0.5–30 μm dense agglomerates of slightly deformed elliptical and mushroom cap shaped particles with no porous structure. Freeze drying resulted in large irregular shape flakes of various sizes ranging mainly between 150 and 350 μm. On the other hand, spray freeze drying of CNC from dilute suspensions ($\sim$ 0.5 wt%) resulted in larger (4–240 μm) light spherical particles that were highly porous ($\sim$ 110 times larger in BET surface area), with web-like inter-connected structure consisting of 10–30 nm thick nanofibrils. Increasing the concentration to 5 wt% produced slightly denser spherical particles (13–110 μm) with slightly less porous web-like structure.

W. Abdallah · M. R. Kamal (✉)
Department of Chemical Engineering, McGill University,
3610 University Street, Montreal, QC H3A 0C5, Canada
e-mail: musa.kamal@mcgill.ca

W. Abdallah
e-mail: wissam.abdallah@mcgill.ca

🍨 Springer

Graphical abstract

Spray Dried CNC   Freeze Dried CNC   Spray Freeze Dried CNC

Introduction

Cellulose nanocrystals (CNC), also referred to as nanocrystalline cellulose or cellulose nanowhiskers, have received great interest owing to their interesting properties such as low density ($\sim$ 1.6 g/cm^3), high tensile strength ($\sim$ 7.5 GPa), high stiffness ($\sim$ 150 GPa), thermal stability up to $\sim$ 300 °C, high aspect ratio (10–100), and low environmental, health, and safety risks (Uhlig et al. 2016), in addition to its projected low cost (Iyer et al. 2015). Moreover, cellulose nanocrystals are derived from biosources, in addition to being biodegradable, biocompatible, abundant and renewable (Mariano et al. 2014). They can be extracted by acid hydrolysis, enzyme treatment, mechanical disintegration, and TEMPO-mediated oxidation (Li et al. 2015) from natural resources, e.g., wood, plants, bacteria, algae (Sacui et al. 2014).

CNC can be used in many potential applications such as filler in polymer nanocomposites to enhance their mechanical, thermal and barrier properties (Habibi et al. 2010; Moon et al. 2011; Rajisha et al. 2014), biocompatible substitutes in biomedical applications such as blood vessel and soft tissue substitutes; skin and bone tissue repair materials; and antimicrobial materials (Jorfi and Foster 2015; Lin and Dufresne 2014; Plackett et al. 2014), foams (e.g., CNC aerogels) for light weight packaging, food packaging, lightweight core-skin structures, and thermal or insulation applications (Ahmadzadeh et al. 2015; Mihindukulasuriya and Lim 2014), rheology modifiers such as polymer melts and particle mixtures to be used in paints, coatings, adhesives, lacquers, drugs, food, cosmetics, and cements (Siqueira et al. 2010), continuous fibers for textile development and long and short fiber-reinforcement applications, hybrid composites with chemical functionality for use in catalysis, biosensors, drug delivery, photovoltaics, and antimicrobial applications (Lin et al. 2012; Moon et al. 2011), barrier films for batteries, and packaging applications (Lin et al. 2012; Moon et al. 2011; Siqueira et al. 2010), optical films or coatings for unique optical patterning of surfaces (Habibi et al. 2010; Siqueira et al. 2010), etc.

The aforementioned applications are affected by the properties of the CNC particles such as morphology and crystallinity. Peng et al. (2013) studied the effect of drying methods (i.e.: air-drying, freeze-drying, spray-drying, and supercritical-drying) on the crystallinity and thermal stability of CNC. According to the rule of mixtures, the mechanical properties of CNC-reinforced composites increase proportionally with crystallinity of cellulose nanocrystals. Meanwhile, the water holding capacity of nanocellulose is related to its crystallinity. When nanocellulose fibrils are included in composites, the absorption of water by cellulose fibrils severely degrades the properties of the composites. The amount of freezing bound water decreases with increasing degree of crystallinity in cellulose fibers (Peng et al. 2013).

Generally, current industrial processes for the production of CNC powders involve the drying of CNC dispersions in water, using spray drying or freeze drying. These processes yield solid, hard, non-porous agglomerates where the nanoparticles adhere to each other due to strong, inter-particle hydrogen bonds. Such agglomerates are difficult to break down and disperse in polymer matrices by melt processing, thus

presenting a serious processing challenge (Zhang et al. 2013). Recently, it was demonstrated that a spray freeze drying (SFD) technique, which combines the advantages of atomization (spraying) and lyophilization (freeze drying) processes yields ultraporous agglomerates of cellulose nanocrystal. Ice crystal growth is the dominant factor in the aggregation process and shrinkage encountered during spray drying is avoided due to the absence of capillary forces (Kamal and Khoshkava 2017; Khoshkava and Kamal 2013). The effect of SFD-CNC particle morphology on dispersion and various properties of polypropylene (Khoshkava and Kamal 2014) and Poly(lactic acid) (Kamal and Khoshkava 2015) nanocomposites was reported. The porous spray freeze dried porous agglomerates with larger BET surface area showed more potential of producing nanocomposites by melt processing than the spray dried or freeze dried agglomerates. Low frequency complex viscosity and storage modulus of polypropylene (PP) were significantly increased by incorporating 5 wt% of SFD-CNC. Moreover, mechanical properties of the nanocomposites were raised, e.g. tensile strength (20% increase) and tensile modulus (43% increase) (Khoshkava and Kamal 2014). These ultraporous homogenous SFD-CNC agglomerates can be used in various applications such as ceramics, catalysts, drug delivery, biomedical scaffolds, etc.

The hydrophilic nature of CNC necessitates its production as an aqueous suspension. This introduces serious transportation-related issues, which can be avoided by drying. Different drying processes yield different agglomerate structures based on how the nanoparticles assemble during the process. The most common drying processes include oven drying, spray drying (SD), freeze drying (FD), supercritical drying and spray-freeze-drying (SFD). In this manuscript, SD, FD and SFD will be considered.

Spray drying is commonly used to produce dry powder from aqueous suspensions (Beck et al. 2012; Peng et al. 2012) due to its relative cost, scalability, and the extensive experience with the spray drying of various materials. In spray drying, a suspension is usually sprayed under high pressure through a pressure multi-nozzle (atomizer) into a flow of hot air (> 100 °C) into a drying chamber, where spiralling droplets encounter a counter-current (or co-current) of hot air which is fed through a diffuser into the chamber (Vicent et al. 2012). This results in micron sized powder agglomerates, determined by water diffusion and evaporation mechanisms (Yoshida et al. 1991).

Freeze drying (lyophilization) is a desiccation process, occurring at low temperature, in which the water in a pre-frozen material sublimes by reducing the surrounding pressure. This process consists of three stages: pre-freezing, primary drying, and secondary drying (Peng et al. 2012). The suspension is frozen in the first step. Then, the pressure is reduced below the triple point of water to allow sublimation to occur, resulting in a dry structurally intact material. After sublimation of the dry ice formed during the primary freeze drying step, secondary drying is necessary to remove the residual bound moisture in the material. This technique is suitable for thermo-sensitive materials, especially for the synthesis of nano-sized powders from inorganic salts and for the manufacture of porous bodies by a freeze-casting process (Moritz and Nagy 2002). An important feature of freeze-drying is that the obtained agglomerates have high porosity. Thus, very light granules can be produced. The porosity and consequently, the density of granules are controlled by the solid loading of the suspensions, whereas the size distribution of the granules is a function of the viscosity and the solid content of the suspension, the flow rate employed for spraying and the pressure of the applied gas (Moritz and Nagy 2002; Vicent et al. 2012).

Spray freeze drying (SFD) is an atomization technique in which an aqueous suspension is atomized (spraying—step I) into a cryogenic liquid such as liquid nitrogen (freezing—step II). This is followed by a second step (freeze drying—step III). In 1980, the Swedish Ceramic Institute (SCI) developed this technique for granulation of ceramic powders (Nyberg et al. 1991). Subsequently, it was used by the food and pharmaceutical industries (Wanning et al. 2015). Besides spraying into a cryo-liquid, spraying and freezing steps can also involve spraying into a cold vapor or spraying into a vapor over cryo-liquid (Hu et al. 2003). During the spraying and freezing stages of the process, suspension droplets freeze as a result of atomization into a cryogenic atmosphere, commonly liquid nitrogen, resulting in larger agglomerate sizes with network structure. On the contrary, in spray drying, suspension droplets shrink during atomization due to the high temperature they encounter. This results in smaller compact particle sizes, compared to spray freeze dried CNC particles. The driving force of

CNC aggregation in the spray drying process is due to the capillary forces. However, in SFD, ice crystal growth controls the process which causes the dispersed phase to collide and aggregate. The cooling rate and droplet concentration in this process influence the size of crystals and growth rate. Meanwhile, the cooling rate depends on droplet size which in turn depends on purging pressure, the flow rate and the distance between the atomizer and liquid nitrogen surface. During spray freezing of CNC suspension in liquid nitrogen, an amorphous ice is formed, and the nanoparticle morphology is frozen-in (Rogers et al. 2002). After freeze drying, a highly porous agglomerate morphology is achieved. Despite the cost and complexity involved in the process, SFD offers prospective applications in high value products i.e. quality, structure, and the retention of volatiles and bioactive compounds (Ishwarya et al. 2015).

Beside the experimental research mentioned above on spray freeze dried CNC, some effort has been carried out to investigate and develop experimental and numerical methods to study the temperature transition of freezing droplets (Hindmarsh et al. 2003). Ishwarya et al. (2015) outlined the principles, methods, significant process parameters, particle morphology and quality aspects of the SFD process together with the recent developments, the application of computational fluid dynamics and mathematical modelling, and the incorporation of new technologies to improve product quality. The main steps in the of many studies focused on the optimization of the last freeze drying step (Liapis and Bruttini 2009; Liu et al. 2008). However, the use of computational fluid dynamics (CFD) tools to simulation of the spray freezing of the SFD technique is still an open promising research area.

The main objective of the present experimental investigation is to study and compare the effects of the above three drying methods (SD, FD, SFD) on some of the important physical characteristics of the dried CNC. The study evaluates the influences of the initial dispersion concentration and batch size on the porosity, BET surface area and WAXD crystallinity of CNC sample. Different concentrations of CNC ranging from ~ 0.5 to 10 wt% were spray-freeze-dried to evaluate concentration effects. Three batch sizes (100 ml, 300 ml and 500 ml) of SFD-CNC were also prepared to study the effects of batch size on the above properties.

Experimental

Preparation of freeze-dried and spray-freeze-dried cellulose nanocrystals

Spray-dried cellulose nanocrystals (SD-CNC), in powder form, were supplied by Forest Products Innovations (FPInnovations, Pointe-Claire, Quebec, Canada). They were used to prepare freeze dried and spray freeze dried CNC (FD-CNC and SFD-CNC). The cellulose nanocrystals in SD-CNC were extracted using sulfuric acid hydrolysis of bleached Canadian softwood Kraft pulp to remove the amorphous cellulose segments. Following removal of residual acid, the protons from the acidic sulfate ester groups were exchanged by neutralization with NaOH to yield a suspension of the sodium form of CNC. The neutral suspension was spray-dried to yield the SD-CNC powder, which was then homogenized by rolling in a clean bottle for 24 h. The average length and thickness of CNC over 150 particles were determined using atomic force microscopy (AFM) and transmission electron microscopy (TEM) as 171 ± 79.7 nm and 15.1 ± 5 nm, respectively (Khoshkava and Kamal 2013).

Few grams of initially spray dried CNC were dispersed in 100 ml of reverse osmosis water using a shear mixer (IKA Works Inc., ultra-turrax T25, Staufen, Germany) and sonicated (Qsonica, Q700, Newtown, CT, USA) for few minutes at room temperature. A probe with a 12.7 mm tip diameter was used at a frequency of 20 kHz and amplitude 2, supplying ca. 750 J/g in order to obtain individual CNC particles by breaking up loosely held agglomerates. An ice bath was used to avoid excessive heating. For FD materials, the suspension was poured slowly in liquid nitrogen and then freeze dried using a 2.5 l freeze drying equipment (Labconco Corp., Kansas City, MO, USA), where the frozen droplets were lyophilized at -52 °C for few days to produce few grams of freeze dried CNC (FD-CNC). For SFD materials, the suspension was sprayed by a spray gun (Campbell Hausfeld DH5300, pattern size 8 in.) into liquid nitrogen (25 ml/min) agitated by a magnetic stirrer bar, using a peristaltic pump. After the spray freezing step, the slurry containing the frozen droplets was transferred to the freeze dryer, where the frozen droplets were lyophilized at -52 °C for few days, yielding a few grams of spray freeze dried CNC (SFD-

CNC). SD-CNC were used as received from the manufacturer. According to the nomenclature used, SFD cellulose nanocrystals (SFD-CNC) samples are identified based on the CNC concentration in the suspension (i.e. for 0.5 mg/100 ml suspensions, SFD-CNC0.5 nomenclature was given). Table 1 lists all the CNC samples prepared.

Characterization of cellulose nanocrystals

Scanning electron microscopy (SEM) and particle size distribution (PSD)

An FEI Inspect F-50 field emission scanning electron microscope (FESEM—FEI company, Hillsboro, OR, USA), operating at low accelerating voltages (2 kV), was used to observe the CNC morphology. The samples were coated with 4 nm thick platinum using an EM ACE600 Leica Microsystems high resolution sputter coater (Concord, ON, Canada) and placed directly without further surface treatment in the SEM chamber. SEM photomicrographs of CNC were taken at 500×, 1500×, 5000× and 25,000× magnifications. Image J software was used to measure the physical dimensions and study the particle size distributions of the CNC agglomerates.

Table 1 Designations of CNC samples

Sample abbreviation	Concentration (wt%)	Volume (ml)
Drying methods		
SD-CNC	–	–
FD-CNC2.0-300	2.0	300
SFD-CNC2.0-300	2.0	300
Concentrations		
SFD-CNC0.5	0.5	100
SFD-CNC1.0	1.0	100
SFD-CNC2.0	2.0	100
SFD-CNC3.0	3.0	100
SFD-CNC4.0	4.0	100
SFD-CNC5.0	5.0	100
SFD-CNC10.0	10.0	100
Batch sizes		
SFD-CNC2.0	2.0	100
SFD-CNC2.0-300	2.0	300
SFD-CNC2.0-500	2.0	500

Adsorption/desorption isotherms and BET surface area

Specific surface areas of starting nanoparticles and their subsequent freeze dried and spray freeze dried agglomerates were determined by multi point N_2 adsorption at − 196 °C, using a TriStar 3000 Surface Area and Porosity Analyzer (static volumetric technique) (Micromeritics Instrument Corp., Norcross, GA, USA) in accordance with the BET (Brunauer–Emmett–Teller) method (Brunauer et al. 1938). In order to determine the adsorption–desorption isotherms, the samples (∼ 150 mg) were outgassed under vacuum for 16 h at 80 °C for CNC. Adsorption/desorption of nitrogen was carried out in the relative pressure range of $0.01 < P/P_o < 1.00$. Specific surface areas were determined from adsorption isotherms by applying the BET formalism in the relative pressure range of $0.05 < P/P_0 < 0.25$. Mesopore analysis was carried out using the Barrett, Joyner and Halenda (BJH) method based on application of the classical Kelvin equation for the estimation of the pore size (Rouquerol et al. 1999).

X-ray diffraction analysis (WAXD)

Wide angle X-ray diffraction (WAXD) analyses were performed at room temperature using a Philips X'Pert Pro X-ray diffractometer (PAnalytical, Almelo, Netherlands) that generates a voltage of 50 kV and current of 40 mA. Approximately 2 mm thick disk-shape samples were used. The X-ray source was a tungsten filament tube with a Cu-target (Kα = 1.5418 Å). The diffraction angle, 2θ, was scanned from 10° to 40° for CNCs at a step size of 0.05°. In order to calculate the basal spacings between the CNC crystalline planes, Bragg's equation was used. The crystallinity indices (CI) of dried CNC samples were calculated using the empirical method described by Segal et al. (2016) and the apparent crystallite size (ACS) of CNC was estimated by broadening of the Debye rings of the Scherrer equation.

Results and discussion

Scanning electron microscopy (SEM) and particle size distribution

Effects of drying methods on morphology

SEM photomicrographs of spray dried CNC (SD-CNC), freeze dried CNC (FD-CNC2.0-300) and spray freeze dried CNC (SFD-CNC2.0-300) taken at 500,

1500, 5000 and 25,000 magnifications are given in Fig. 1, and their particle size distributions analyzed using the histograms generated from SEM micrographs are summarized in Table 2.

Spray drying of CNC produced nonporous, densely packed agglomerates of slightly deformed ellipsoidal shapes resulting from shrinkage due to capillary forces in the process of spray drying, as seen in the SEM micrographs of Fig. 1a. The particle sizes of the resulting spray dried agglomerates SD-CNC varied
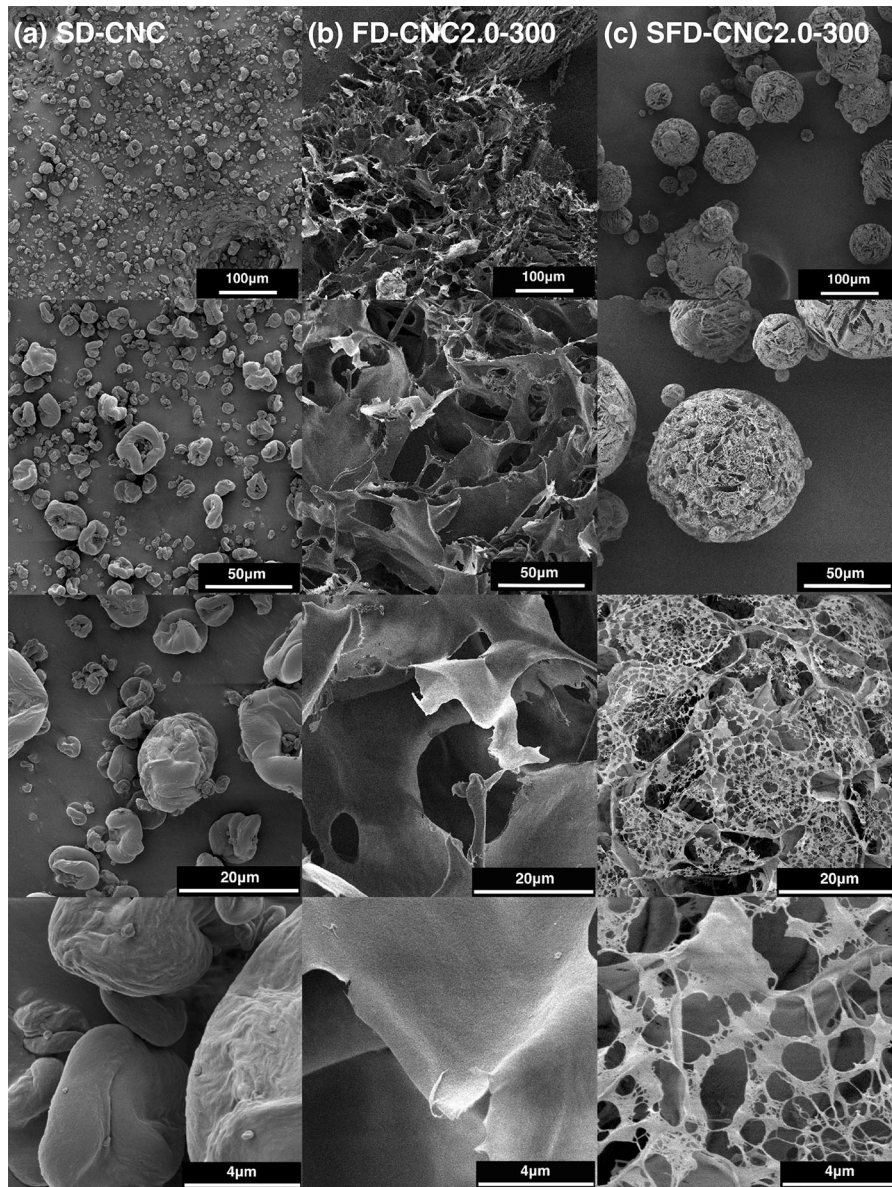
Fig. 1 SEM micrographs of CNC agglomerates at different magnifications ×500, ×1500, ×5000, ×25,000 **a** SD-CNC, **b** FD-CNC2.0-300, **c** SFD-CNC2.0-300

Table 2 Particle size distribution extracted from SEM images using imageJ software

Sample	Particle size distribution (μm)	d90 90% of particles are less than (μm)	d50 50% of particles are less than (μm)	Main distribution (μm)	Median (μm)	Mean (μm)
Drying methods						
SD-CNC	0.5–30	10	4	0.5–10	3	5
FD-CNC2.0-300	150–20,000	–	–	150–350	–	–
SFD-CNC2.0-300	4–184	88	29	5–80	30	39
Concentrations						
SFD-CNC0.5	7–143	82	36	10–80	35	42
SFD-CNC1.0	21–237	140	75	20–120	78	81
SFD-CNC2.0	14–190	101	41	20–80	41	54
SFD-CNC3.0	8–168	99	33	20–80	34	44
SFD-CNC4.0	6–225	139	30	10–100	32	51
SFD-CNC5.0	13–111	99	44	20–80	47	49
SFD-CNC10.0	4–135	49	14	6–50	11	21
Batch sizes						
SFD-CNC2.0	14–190	101	41	20–80	41	54
SFD-CNC2.0-300	4–184	88	29	5–80	29	39
SFD-CNC2.0-500	11–209	92	35	15–80	34	46

between 0.5 and 30 μm with main distribution ranging between 0.5 and 10 μm, with 90% of the samples smaller than 10 μm and the mean particle size was ~ 5 μm. In spray drying of CNC samples, shrinkage occurs due to the presence of capillary forces. The surface of the droplets dries upon contacting the hot air atmosphere. Then, water diffuses from the inner core towards the surface. The evaporation of water at the surface of the droplets and diffusion of inner-layer water towards the surface of the droplet compete to define the final morphology of the dry particle. The rate of diffusion is usually slower than the evaporation rate. Thus, a gradient occurs in the aggregation structure of the final particle. The resultant shape of the spray dried aggregated particles is usually a compact ellipsoidal powder, due to capillary forces.

FD-CNC2.0-300 exhibits porous and large irregularly shaped flakes of various sizes ranging between 150 and 350 μm. In freeze drying of CNC samples, the shrinkage occurring during spray drying is avoided due to the absence of capillary forces. In freeze drying ice crystal growth is the dominant factor in the aggregation process. Thus, CNC particles collide and aggregate due to ice formation. In freeze drying process, ice formation and growth rate are the determine CNC aggregation. Freeze drying of the

CNC suspension yields large thin particles (> 100 μm) with very limited porosity (Beck et al. 2012; Peng et al. 2012). FD-CNC2.0-300 had very similar morphology to those of Peng et al. (2012).

Spray freeze drying of CNC from suspensions with low concentrations produced highly porous and larger agglomerates with sizes between 4 and 184 μm, with the main distribution in the range between 5 and 80 μm and the mean size of the particles was ~ 39 μm (Fig. 1c). SFD-CNC has a porous structure consisting of an assembly of flat and thin walls. Very small droplets loaded with nanoparticles and having a broad droplet size distribution freeze in liquid nitrogen immediately. They maintain the broad size distribution and freeze the cellulose particle configuration within the drop. Upon drying, the resulting cellulose agglomerates will form a network of nanoparticles, which almost maintains the nanoparticle networks and the size and shape of the original droplets. The shrinkage that dominates the spray drying process is avoided by using the FD or SFD techniques, due to the absence of capillary forces and because ice crystal growth is the dominant factor in the SFD process. The properties of freeze-dried or spray-freeze-dried products are strongly influenced by the freezing rate before the drying process. A slow freezing rate favors the

formation of elongated ice crystals. During their growth, the ice crystals can move and bring CNC nanoparticles closer to each other and to change pore structures in solid agglomerates. With increasing freezing rate the growth of the ice crystals is reduced and, at very high freezing rates, crystallization can be suppressed. Nevertheless, a recrystallization of the amorphous ice can occur in the frozen state at elevated temperatures, for instance during the storage of frozen products in a refrigerator (Meryman 1957).

The spray freeze drying process is described in literature for several materials, for instance alumina powders and other ceramic materials, calcium phosphate powders, protein inhalation powders for pharmaceutical applications or proteins (Moritz and Nagy 2002). In very fast cooling, such as spraying under liquid nitrogen, an amorphous ice could be formed and nanoparticle morphology would be frozen and very highly porous structure is usually obtained (Rogers et al. 2002).

Granulates of nano-sized powders prepared by a spray freezing technique show preserved homogeneity and yield a spherical granule shape, increased bulk and tap density, improved flowability, and a reduced amount of dust (Wang et al. 2012). In comparison to conventionally spray dried granulates, spray freeze dried granulates are much weaker, because capillary forces can be excluded in this technique. The properties of the granulates are influenced by the suspension viscosity, the solid content, geometric parameters of the atomizing nozzle and the freezing rate.

## Effects of suspension concentrations on morphology

Figure 2 shows SEM photomicrographs of spray freeze dried CNC prepared from different concentrations (0.5, 1.0, 2.0, 3.0, 4.0, 5.0 and 10.0 wt%) at different magnifications. Particle size distribution results generated from the SEM micrographs are summarized in Table 2 and Fig. 3.

Spray freeze drying of CNC starting from dilute suspensions (i.e. ∼ 0.5%) resulted in small spherical, very fluffy and highly porous agglomerates consisting of interconnected with 10–30 nm thick nanofibrils (Fig. 2a) compared to the relatively larger particles prepared from high concentration suspensions (i.e. ∼ 1.0–5.0%) (Fig. 2b–f). The particle sizes of SFD-CNC0.5 particles ranged between 7 and 143 μm and they were mainly distributed between 10 and 80 μm.

The mean size of the particles was 42 μm. On the other hand, increasing the concentration of the suspension slightly to 1.0 wt% (SFD-CNC1.0) resulted in larger and more fluffy and porous agglomerates of sizes ranging between 21 and 237 μm and mainly distributed between 20 and 120 μm, and the mean size of the particles increased to 81 μm. (Figure 2b). The thickness of the nano-fibrils connecting the pores in SFD-CNC1.0 remained in the 10–30 nm range of as for SFD-CNC0.5. Increasing the concentration of the suspension to 2.0 wt% (SFD-CNC2.0) reduced the particles size without compromising the porous structure and the mean size of the particles decreased to 54 μm. (Figure 2c). This mean fluctuated slightly between 44 and 54 μm for SFD-CNC3.0 (Fig. 2d), SFD-CNC4.0 (Fig. 2e) and SFD-CNC5.0 (Fig. 2f). The thickness of the nanofibrils connecting the pores in SFD-CNC2.0 SFD-CNC3.0, SFD-CNC4.0 and SFD-CNC5.0 increased with concentration and ranged between 20 and 50 nm. High concentration of SFD-CNC10.0 resulted in the smallest agglomerates (mean of 21 μm) compared to less-concentrated suspensions (between 0.5 and 5%). Spherical particles were obtained, featuring highly dense agglomerates with limited porosity and particle sizes between 4 and 135 μm mainly distributed between 6 and 50 μm (Fig. 2g). The 10% suspension resulted in less porous structure. Effects of Suspension Batch Size on Morphology.

Figure 4 shows SEM photomicrographs of SFD-CNC at 2 wt% concentrations prepared in three different batch sizes 100 ml (SFD-CNC2.0), 300 ml (SFD-CNC2.0-300) and 500 ml (SFD-CNC2.0-500). Particle size distribution results generated from SEM micrographs for these samples are summarized in Table 2. Spray freeze drying of 2% CNC suspensions resulted in similar agglomerates using the three different batch sizes. The agglomerate sizes of SFD-CNC2.0, SFD-CNC2.0-300, and SFD-CNC2.0-500 (Fig. 4) varied between 4 and 209 μm mainly distributed between 5 and 80 μm. The batch size had small influence on the particle size distribution. This suggests that the preparation of SFD-CNC from larger batches (100–500 ml) will likely yield similar products.
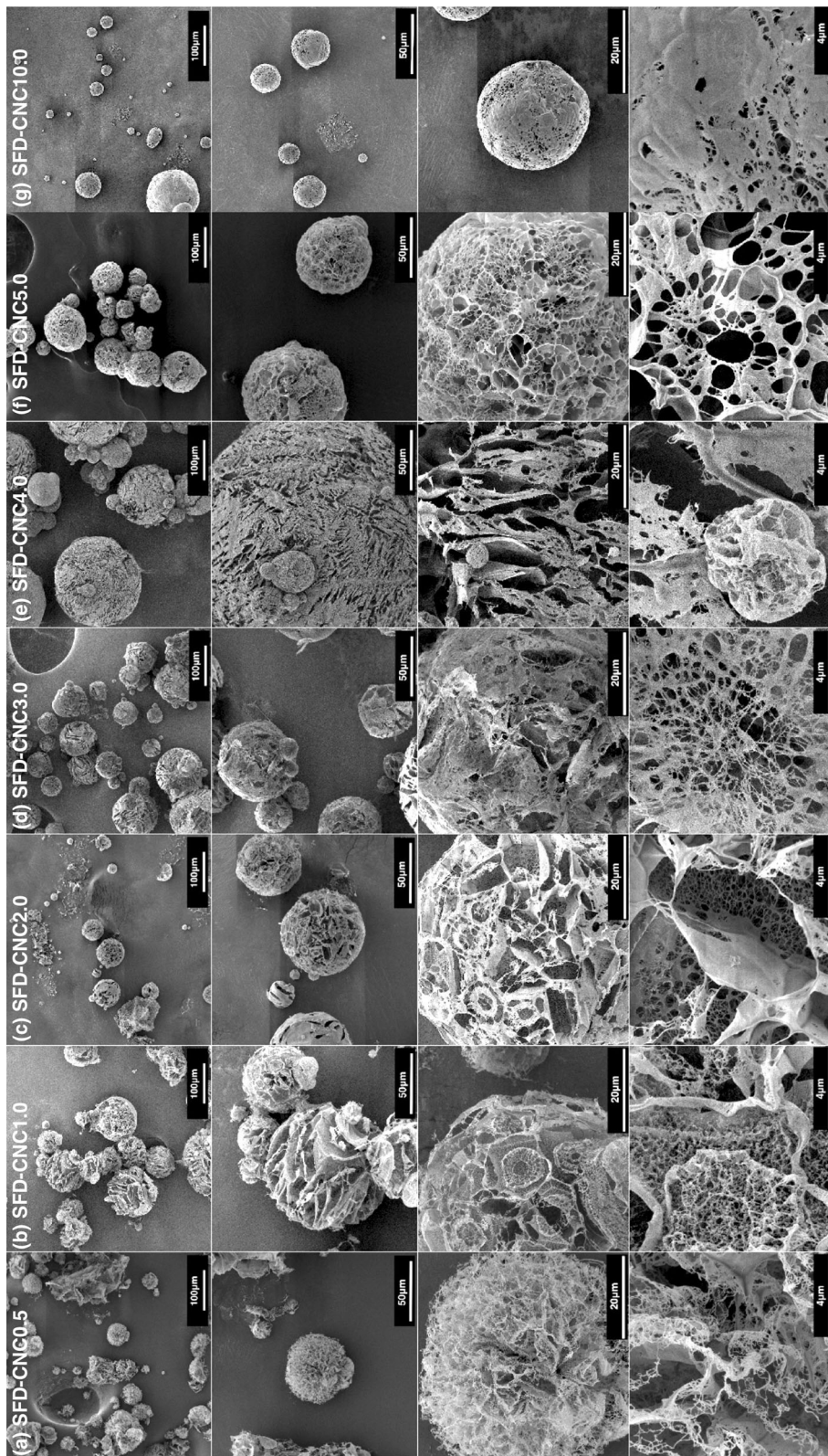
Fig. 2 SEM micrographs of CNC agglomerates at different magnifications ×500, ×1500, ×5000, ×25,000 **a** SFD-CNC0.5, **b** SFD-CNC1.0, **c** SFD-CNC2.0, **d** SFD-CNC3.0, **e** SFD-CNC4.0, **f** SFD-CNC5.0, **g** SFD-CNC10.0
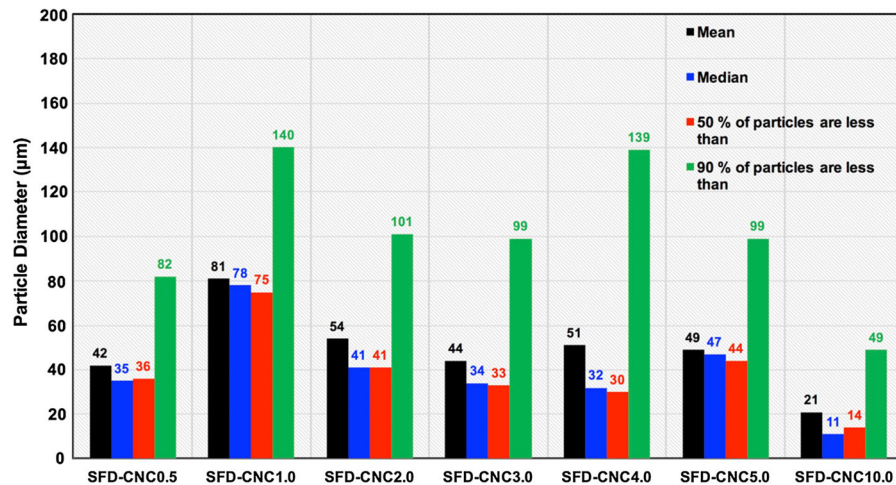
Fig. 3 Particle size distribution diagram of CNC agglomerates prepared from different concentrations: SFD-CNC0.5, SFD-CNC1.0, SFD-CNC2.0, SFD-CNC3.0, SFD-CNC4.0, SFD-CNC5.0 and SFD-CNC10.0

Adsorption/desorption isotherms and BET surface area of CNC samples

SEM provided us with a qualitative insight into the texture of the CNC agglomerates for spray-dried, freeze-dried and spray-freeze-dried samples. Pore size analyses based on SEM images using image J software can provide an approximate qualitative porosity analysis. However, adsorption/desorption isotherms provide a dependable quantitative analysis of the porosity of agglomerates. The measurements of nitrogen adsorption/desorption isotherms were carried out in order to assess the changes of the specific surface areas in the investigated CNC particles. The data extracted from the isotherms of all samples are given in Table 3.

Pores are characterized according to their sizes: Pores > 50 nm in diameter are called macropores. Pores 2–50 nm in diameter are called mesopores and pores < 2 nm in diameter are called micropores (Rouquerol et al. 1994). According to IUPAC classification, all CNC isotherms can be classified as type IV accompanied by type H3 hysteresis, typical of mesoporous region (Rouquerol et al. 1999) and coherent with earlier analysis on CNC (Sing 1985). Table 3 shows the specific total surface area (S_{BET}) calculated using the BET method in the range $0.05 < P/P_o < 0.2$ for all CNC particles.

The average pore width is usually obtained by the Gurwitch rule: $D = 4 V/S_{BET}$ where D is the average pore diameter, V is the total pore volume and S_{BET} the

specific surface area usually obtained using the BET model. This geometrical relationship is based on some assumptions that pores must be homogeneous in diameter, cylindrical and rigid.

BJH method is based on geometric calculations of species being desorbed at given relative pressures. This model requires the Kelvin law, which relates the relative pressure at which condensate gas will evacuate pores satisfying this equation. This model also requires a relationship between the relative pressure and the thickness of the adsorbed multilayer. This can be represented by the Harkins and Jura equation, but others may apply. S_{BET} is given by BET equation, which is the same in calculation of average pore diameter by BET and BJH. The difference is that the volumes V used in these two methods are different: (a) by BET, V is a single point volume which generally is the total volume less than the largest P/P_0; (b) by BJH, V is a definitive volume which represents a volume at a range of P/P_0 (or at a range of pore diameters). Thus, the average pore diameter by BET and BJH is different based on their limiting conditions.

The CNC particle physical analysis depends on multiple factors; (1) particle shape (morphology) (2) particle size, (3) surface texture (pore size, pore volume, pore shape [geometry], pore size distribution [connectivity]) and (4) surface area.
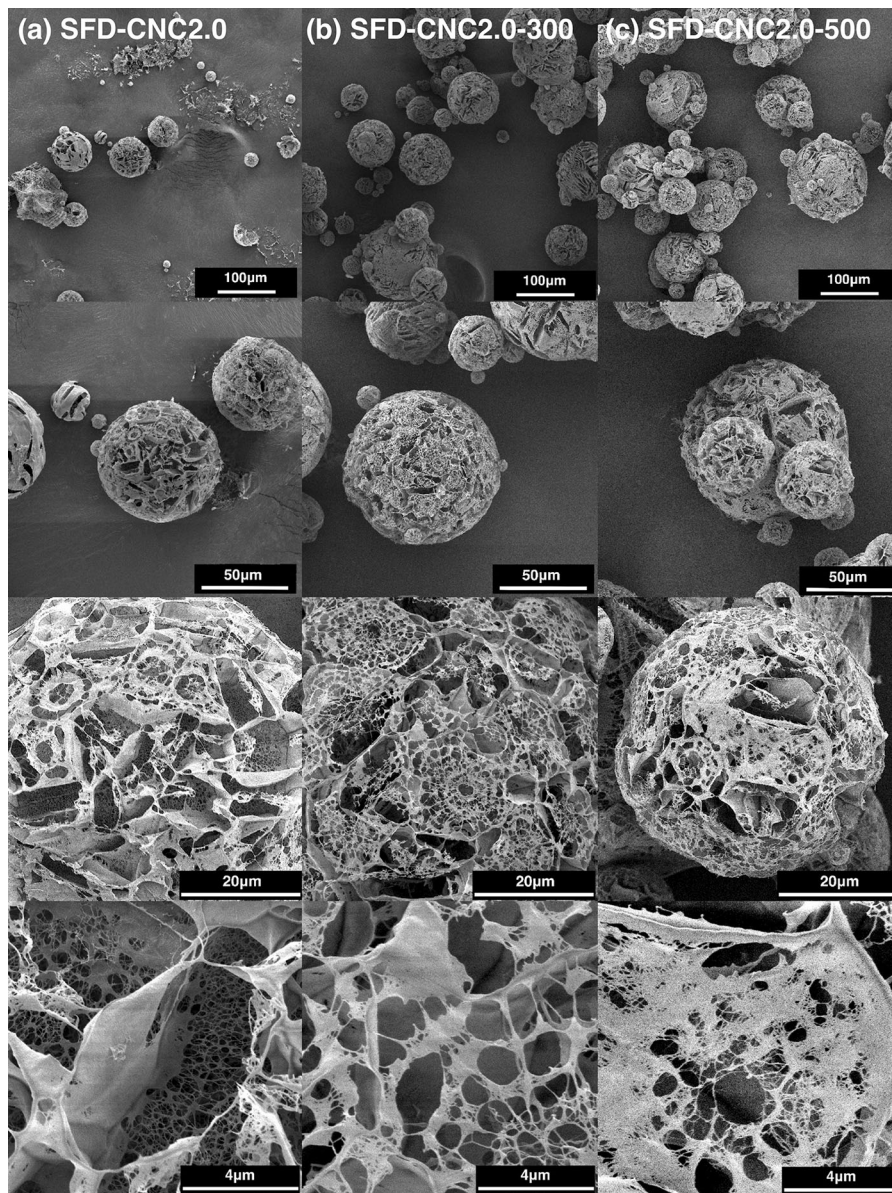
Fig. 4 SEM micrographs of CNC agglomerates at different magnifications ×500, ×1500, ×5000, ×25,000 of **a** SFD-CNC2.0-100, **b** SFD-CNC2.0-300, **c** SFD-CNC2.0-500

Effects of drying methods on adsorption properties

The measurements of nitrogen adsorption/desorption isotherms were carried out in compare the possible changes of the specific surface areas in the investigated CNC particles using different drying procedures (Fig. 5a). The data extracted from the isotherms of spray dried CNC, freeze dried CNC (FD-CNC2.0-

300) and spray freeze dried CNC (SFD-CNC2.0-300) are given in Table 3.

Surface area is related to particle geometry (morphology), particle size, surface texture and porosity. It shows that the specific total surface area calculated using the BET method in the range $0.05 < P/P_o < 0.2$. SD-CNC has the lowest value of S_{BET} (0.5 m^2/g). This value increases from 0.5 to 17.2 m^2/g (corresponding to an increase of $\sim$ 34 times) for FD-CNC2.0-300

Table 3 Numerical results derived from the BET and BJH methods of the N_2 adsorption–desorption isotherms

Sample	BET	BJH adsorption			BJH desorption		
	S_{BET} (m²/g)	$S_{BJH-Ads.}$ (m²/g)	$V_{P-Ads.}$ (cm³/g)	$r_{P-Ads.}$ (nm)	$S_{BJH-Des.}$ (m²/g)	$V_{P-Des.}$ (cm³/g)	$r_{P-Des.}$ (nm)
Drying methods							
SD-CNC	0.5	0.19	0.0032	66.7	0.23	0.0033	57.9
FD-CNC2.0-300	17.2	15.15	0.0723	19.1	15.95	0.0730	18.3
SFD-CNC2.0-300	56.4	48.70	0.1635	13.4	48.70	0.1638	13.4
Concentrations							
SFD-CNC0.5	70.2	63.32	0.2825	17.8	63.98	0.2838	17.7
SFD-CNC1.0	77.2	61.98	0.2183	14.1	60.45	0.2193	14.5
SFD-CNC2.0	56.4	48.50	0.1574	13.0	48.74	0.1575	12.9
SFD-CNC3.0	45.0	34.84	0.1163	13.4	34.27	0.1174	13.7
SFD-CNC4.0	29.8	26.16	0.1123	17.2	26.08	0.1126	17.3
SFD-CNC5.0	20.5	15.49	0.0669	17.3	14.29	0.0669	18.7
SFD-CNC10.0	28.1	23.89	0.116	19.4	23.39	0.1160	19.9
Batch sizes							
SFD-CNC2.0	56.4	48.50	0.1574	13.0	48.74	0.1575	12.9
SFD-CNC2.0-300	56.4	48.70	0.1635	13.4	48.70	0.1638	13.4
SFD-CNC2.0-500	58.7	49.72	0.1583	12.7	50.09	0.1586	12.7

S_{BET} BET surface area, $S_{BJH-Ads.}$ BJH adsorption cumulative surface area of pores between 1.7 and 300 nm width, $V_{P-Ads.}$ BJH adsorption cumulative volume of pores between 1.7 and 300 nm width, $r_{P-Ads.}$ BJH adsorption average pore width (4 V/A), $S_{BJH-Des.}$ BJH desorption cumulative surface area of pores between 1.7 and 300 nm width, $V_{P-Des.}$ BJH desorption cumulative volume of pores between 1.7 and 300 nm width, $r_{P-Des.}$ BJH desorption average pore width (4 V/A)

prepared via freeze drying. The BET surface area was 13.4 m²/g for FD-CNC0.75 prepared by Lu and Hsieh (2010). It is important to note that the freeze drying process can result in different surface areas depending on the initial concentration, suspension stability, etc. On the other hand, spray freeze drying of the same suspension resulted in a significant increase in S_{BET} to 56.4 m²/g (corresponding to an increase of $\sim$ 113 times compared to SD-CNC). This increase in the BET surface area is clearly reflected in the highly porous web-like interconnected structure of the SEM images (Fig. 1).

Table 3 reveals that SFD-CNC2.0-300 sample exhibits higher adsorption of nitrogen compared to SD-CNC and FD-CNC2.0-300 throughout all the relative pressures ($P/P_o < 1.0$). The increase of nitrogen sorption from very low to medium relative pressure ($P/P_o < 0.4$) indicates the increase in the proportion of micropores and small mesopores. The increase of the nitrogen adsorbed at higher relative pressures can be related to the formation of larger mesopores and small macropores due to the strong delamination as a consequence of the synthetic

conditions of the porous SFD-CNC2.0-300 leading to a web-like structures. This result suggests that the addition of more solid particles in larger concentrated suspensions has a negative influence on the amount of micropores and small mesopores.

While the overall appearance of the plots is similar (Fig. 5a), the amount of nitrogen adsorbed on SD-CNC surface ($\sim$ 3 cm³/g) is substantially smaller than on those of FD-CNC2.0-300 ($\sim$ 50 cm³/g) and SFD-CNC2.0-300 ($\sim$ 110 cm³/g) samples.

The cumulative pore volume from BJH calculations, V_{P-Ads} in SFD-CNC2.0-300 increased significantly (0.1635 cm³/g: $\sim$ 51 times larger) and FD-CNC2.0-300 (0.0723 cm³/g: $\sim$ 23 times larger) compared to the original SD-CNC (0.0032 cm³/g). This gives clear insight about the porous structure of CNC after spray freeze drying allowing more nitrogen to accumulate during the sorption process. The smaller cumulative pore volume of the spray dried cellulose nanocrystals is expected due to the rigid and highly hydrogen bonded cellulose structures. The pore volume of spray-freeze-dried cellulose nanocrystals increased after loosely packed structures took shape

Fig. 5 Nitrogen
adsorption/desorption
isotherms at 77 K of **a** SD-
CNC, FD-CNC2.0-300 and
SFD-CNC2.0-300, **b** SFD-
CNC0.5, SFD-CNC1.0,
SFD-CNC2.0, SFD-
CNC3.0, SFD-CNC4.0,
SFD-CNC5.0 and SFD-
CNC10.0, **c** SFD-CNC2.0-
100, SFD-CNC2.0-300 and
SFD-CNC2.0-500
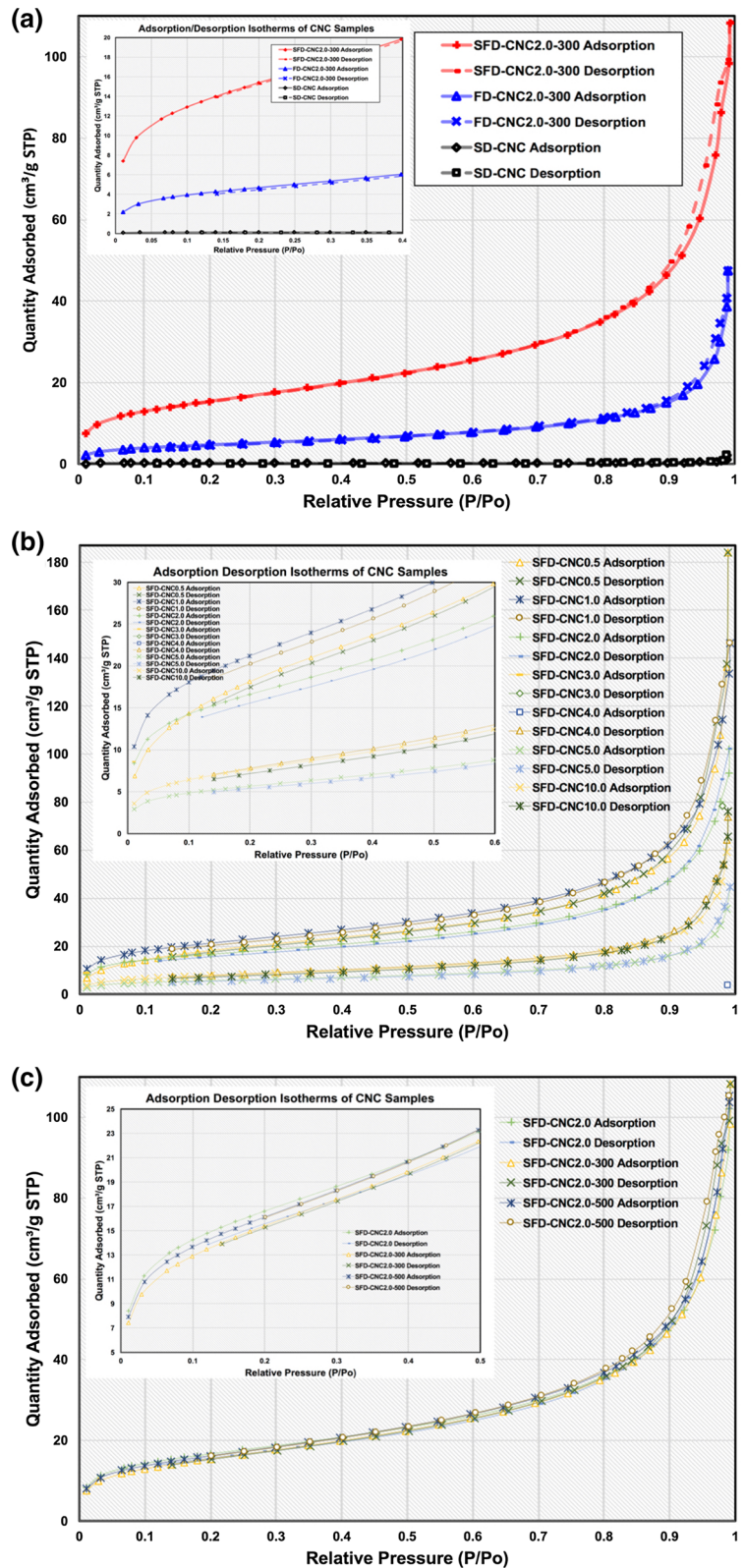
to create a very large number of mesopores among the nanocrystals.

The same trend was observed with cumulative surface area of pores for spray dried and spray-freeze-dried cellulose nanocrystals, but with much larger differences. The cumulative pores surface area of the spray-freeze-dried cellulose nanocrystals SFD-CNC0.5 (63.32 m^2/g) was 333 times the original spray-dried cellulose powder SD-CNC (0.19 m^2/g). While the original spray dried cellulose nanocrystals possessed 0.39 m^2/g micropores in its structure, the negative Y-intercept calculated in t-plot (not shown here) for spray-freeze-dried cellulose nanocrystals indicated absence of micropores. When the micropore area is not reported (in other words the Y-intercept is negative), it is because either the micropore volume is negative or the calculated external surface area is larger than the total surface area. This result suggests that aggregation by strong hydrogen-bonding effect in spray-drying could be significantly reduced in freeze drying and spray freeze-drying. This conclusion was further evidenced by the $\sim$ 130 times higher BET surface area of SFD-CNC0.5 (70.2 m^2/g) compared to the spray-dried SD-CNC (0.5 m^2/g).

In the meantime, the BJH pore radius decreases from 66.7 nm for SD-CNC to 19.1 nm and 13.4 nm for FD-CNC2.0-300 and SFD-CNC2.0-300, respectively. This clearly shows how spray freeze drying in SFD-CNC2.0-300 induced smaller pore sizes and resulted therefore in higher surface areas. This suggests that the structure in the spray-freeze-dried cellulose nanocrystals is mesoporous. However, for spray dried CNC, the pore width was the largest because of its nonporous structure since BJH model could detect the large voids among the compacted aggregates as the pores.

Effects of suspension concentrations on adsorption properties

The nitrogen adsorption/desorption isotherms are given in Fig. 5b for spray freeze dried CNC prepared from suspensions with the different concentrations.

S_{BET} increases (from 0.5 to 70.2 m^2/g) with spray freeze drying 0.5 g SD-CNC in 100 ml of reverse osmosis water (SFD-CNC0.5), indicating over two orders of magnitude increase in the surface area, which is also evident from the porous texture observed in SEM images. SFD-CNC0.5 and SFD-CNC1.0

exhibited the largest S_{BET} of 70.2 and 77.2 m^2/g, respectively, and then decreased gradually as the concentration of CNC in the system increased from SFD-CNC2.0 (56.4 m^2/g) to 5.0 to SFD-CNC5.0 (20.5 m^2/g), respectively. This decrease can be related to the observed contraction in the fibrilous structure and the partial filling of the pore volume. SFD-CNC10.0 exhibited slightly higher S_{BET} of 28.1 m^2/g compared to SFD-CNC5.0.

The cumulative pore volumes from BJH calculations, $V_{P\text{-}Ads}$ of all SFD-CNC samples varied in a manner similar to the BET surface area, with values ranging between 0.0669 and 0.2825 cm^3/g. The average pore widths ranged between 13.0 and 19.4 nm. The mesopores, which had a measured mean pore width of $\sim$ 13–19 nm, are much smaller than the amorphous pores in the original spray dried cellulose nanocrystals with a mean pore width of 66.7 nm. It is possible that the mesopores existed as the inter-crystal voids resulting from the sublimation of ice crystals and the corresponding driving force to move isolated cellulose nanocrystals closer. The same trend was observed with cumulative surface area of pores for spray-freeze-dried cellulose nanocrystals of all concentrations.

Effects of suspension batch sizes on adsorption properties

Figure 5c shows that the isotherms of SFD-CNC prepared from batches 100 ml, 300 ml and 500 ml have no significant difference. Moreover, the data extracted in Table 3 show almost no difference in S_{BET} (56.4–58.7 m^2/g). This is also clear in the practically identical structure seen in the corresponding SEM micrographs (Fig. 4). This suggests that the production of SFD-CNC from larger batches will not compromise the quality of the final product and indicates that this procedure is likely to be scalable to meet industrial needs using appropriate equipment.

The cumulative pore volume from BJH calculations, $V_{P\text{-}Ads}$ in all SFD-CNC2.0 batches was around 0.1600 cm^3/g. The same trend was observed with the cumulative surface area of pores ($\sim$ 49.0 m^2/g) as well as the pore sizes ($\sim$ 13.0 nm).

Table 4 Numerical results (d spacing, CI and ACS) derived from the WAXD diffractograms for SD-CNC, FD-CNC and SFD-CNC

Sample	Basal Spacing (nm)			Crystallinity index (%)	Apparent crystallite size[a] (nm)
	$(1\bar{1}0)$	(110)	(200)		
Drying methods					
SD-CNC	0.588	0.541	0.397	90.9	3.756
FD-CNC2.0-300	0.594	0.533	0.398	84.8	3.301
SFD-CNC2.0-300	0.604	0.551	0.403	84.2	4.128
Concentrations					
SFD-CNC0.5	0.618	0.533	0.396	84.9	4.218
SFD-CNC1.0	0.629	0.550	0.399	81.8	4.462
SFD-CNC2.0	0.596	0.545	0.398	83.9	4.276
SFD-CNC3.0	0.604	0.545	0.399	86.5	3.966
SFD-CNC4.0	0.600	0.560	0.399	86.3	4.053
SFD-CNC5.0	0.600	0.540	0.399	87.3	3.860
SFD-CNC10.0	0.593	0.535	0.397	87.4	3.670
Batch sizes					
SFD-CNC2.0	0.596	0.550	0.398	83.9	4.276
SFD-CNC2.0-300	0.604	0.551	0.403	84.2	4.128
SFD-CNC2.0-500	0.618	0.535	0.401	86.9	4.278

[a]Uncertainty represents the standard deviation of replicate measurements (n = 3) from calculations based on the (200) reflection plane peak

X-ray diffraction analysis

Cellulose nanocrystals contain chains with both crystalline (ordered) and amorphous (less ordered) regions, as described by the traditional two-phase cellulose model (Park et al. 2010). The major diffraction peaks at $2\theta = 14.8°$, 16.3°, 22.45° and 34.5° were assigned as the crystalline planes with Miller indices of $1\bar{1}0$, 110, 200 and 004 in the crystal structure of cellulose I (Nishiyama et al. 2002). The corresponding basal spacings (d) of the crystalline planes ($1\bar{1}0$, 110, 200) calculated using Bragg's Eq. (1) are given in Table 4:

$$n\lambda = 2d\sin\theta \qquad (1)$$

where n is an integer, λ is the wavelength of incident wave (1.5418 Å), and θ is the angle between the incident ray and the scattering plane.

The crystallinity index (CI) was used to describe the relative amount of crystalline material in the CNC samples prepared using different drying methods, concentrations and batch sizes. The crystallinity index of dried cellulose nanocrystal samples was calculated using the empirical method described by Segal et al. (2016). The height ratio between the intensity of the crystalline peak $(I_{200} - I_{am})$ and total intensity (I_{200}) after subtracting the baseline (Cao and Tan 2005; Segal et al. 2016) as given in Eq. (2):

$$CI\,(Crystallinity\,Index) = \frac{I_{200} - I_{am}}{I_{200}} \times 100 \qquad (2)$$

where I_{200} is the maximum intensity of the principal peak (200) lattice diffraction corresponding to both crystalline and amorphous material at $2\theta \sim 22.45°$ for cellulose I, and I_{am} is the intensity of diffraction attributed to amorphous cellulose, the minimum between the I_{110} peak and the I_{200} peak (at $2\theta \sim 18.5°$ for cellulose I) (French and Santiago Cintrón 2013; Segal et al. 2016).

Apparent crystallite size (ACS) of CNC was estimated by broadening of the Debye rings of the Scherrer Eq. (3):

$$Apparent\,Crystallite\,Size\,(ACS) = \frac{0.89 * \lambda}{\beta\cos\theta} \qquad (3)$$

where λ is the wavelength of the incident X-ray (1.5418 Å), θ is the Bragg angle corresponding to the (200) plane, and β is the full width at half maximum (FWHM) of the broad diffraction line of the (200) reflection in radians.

Fig. 6 WXRD
diffractograms of CNC
agglomerates: **a** SD-CNC,
FD-CNC2.0-300 and SFD-
CNC2.0-300, **b** SFD-
CNC0.5, SFD-CNC1.0,
SFD-CNC2.0, SFD-
CNC3.0, SFD-CNC4.0,
SFD-CNC5.0 and SFD-
CNC10.0 and **c** SFD-
CNC2.0, SFD-CNC2.0-300
and SFD-CNC2.0-500
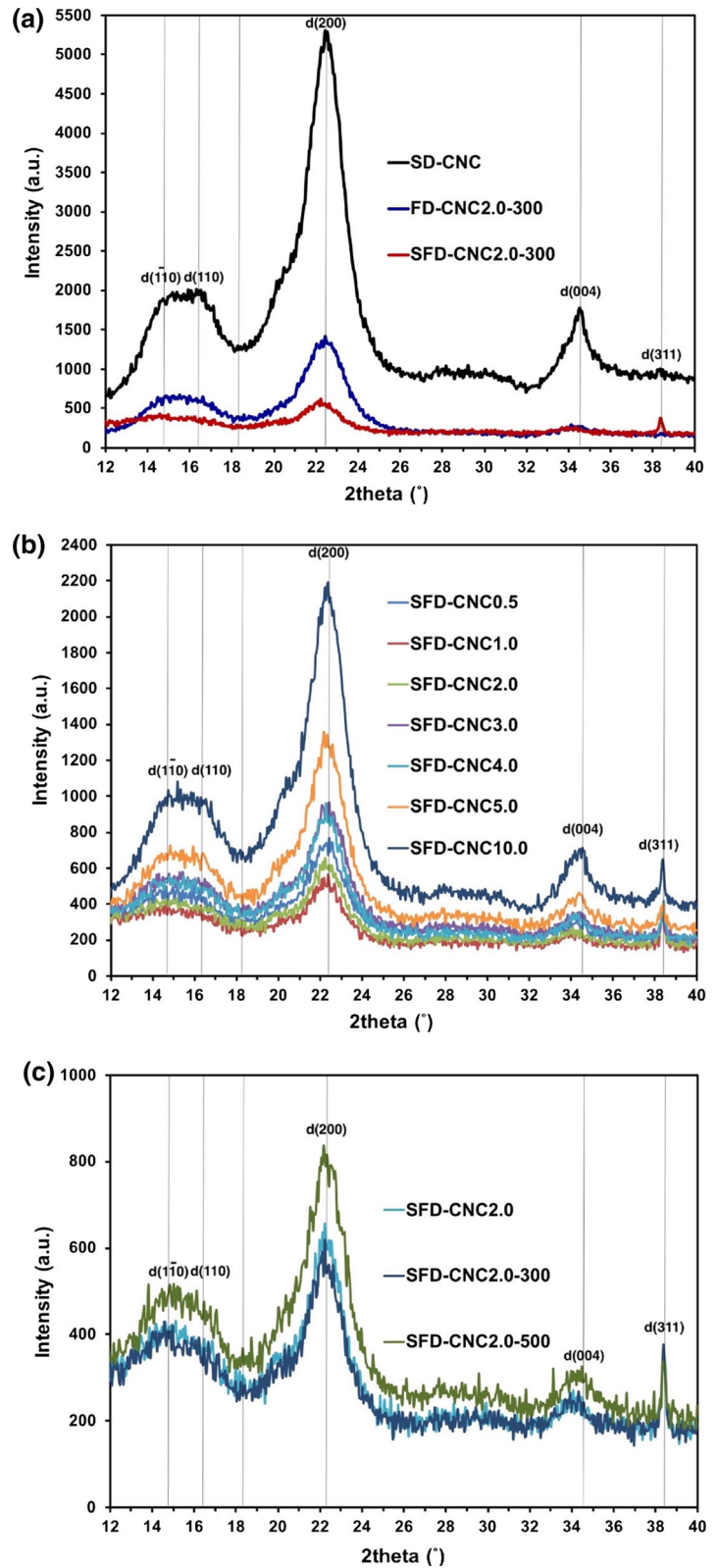
In order to smooth out the effect of noise in the diffractogram, FWHM and peak position for the (200) reflection were determined from the fitted diffractograms using a Gaussian function for 2θ. The signal intensity however was found from the original diffractogram to avoid de-convoluting the (200) diffraction peak profile. (Agarwal et al. 2017).

Effects of drying methods on crystalline structure

The X-ray diffraction patterns of spray dried CNC, freeze dried CNC (FD-CNC2.0-300) and spray freeze dried CNC (SFD-CNC2.0-300) are shown in Fig. 6a.

Table 4 lists the crystallinity index and apparent crystallite size of SD-CNC, FD-CNC2.0-300 and SFD-CNC2.0-300. The crystallinity index of the SD-CNC was the highest at 90.9%. The high crystallinity of SD-CNC can be attributed to the heat treatment of the CNCs (Peng et al. 2013; Yildiz and Gümüşkaya 2007) and the recrystallization of amorphous cellulose, observed with heat and humidity during the spray drying process (Hatakeyama and Hatakeyama 1981; Peng et al. 2013). CI decreased in the case of FD-CNC2.0-300 (84.8%) and SFD-CNC2.0-300 (84.2%). The crystallinity index for FD-CNC2.0-300 was slightly higher than the value (82%) reported by Li et al. (Li et al. 2011). The apparent crystallite sizes for SD-CNC, FD-CNC2.0-300 and SFD-CNC2.0-300 were 3.76 nm, 3.30 nm and 4.13 nm, respectively. Freeze dried and spray freeze dried CNC prepared from 2 wt% in 300 ml batches showed close crystallinity indices whereas SFD-CNC2.0-300 showed the highest apparent crystallite size of 4.13 nm compared to the other drying methods. The lower crystallinity index for FD-CNC2.0-300 and SFD-CNC2.0-300 can be attributed to the free ordering of cellulose nanocrystals, forming samples with lower crystallinity compared to spray dried samples.

Effects of concentrations on crystalline structure

The X-ray diffraction patterns of spray freeze dried CNC prepared from different suspension concentrations (0.5, 1.0, 2.0, 3.0, 4.0, 5.0 and 10.0 wt%) are given in Fig. 6b.

The crystallinity indices of SFD-CNC samples prepared at different concentrations increased with concentration and varied between 81.8% for SFD-CNC1.0 up to 87.4% which is relatively in correlation with the increase in porosity for low concentration suspensions, with the exception of SFD-CNC0.5 which exhibited slightly higher CI compared to SFD-CNC2.0. For samples prepared under non-aqueous conditions or highly concentrated solutions of cellulose, hydrogen bonding can occur directly among the hydroxyl groups of the cellulose chains. This hydrogen bonding brings cellulose nanofibrils close together to form firm aggregates resulting in the formation of crystalline structures (Wanning et al. 2015). The ultra-sonication step allows the particles to break down to the nanoscale and the spray freezing step in liquid nitrogen allows these nanoparticles to agglomerate in the form of crystals. The ultra-sonication step induces change in the structure of crystallites such as folding, surface erosion, and fibrillation (Peng et al. 2013). In freeze drying, the suspension freezes within liquid nitrogen without spraying. During spray freeze drying, however, the spray freezing step involves spraying fine particles within water droplets from the nozzle which instantaneously freeze in liquid nitrogen and maintain the individual particle structure which then dries in the freeze dryer. This step allows the particles to agglomerate individually in which hydrogen bonding can occur directly among the hydroxyl groups of the cellulosic chains. The hydrogen-bonding drives cellulose nanocrystals to approach each other and form tight aggregates resulting in the formation of crystalline structures.

Effects of batch sizes on crystalline structure

The X-ray diffraction patterns of spray freeze dried CNC prepared from different concentrations (0.5, 1.0, 2.0, 3.0, 4.0, 5.0 and 10.0 wt%) are given in Fig. 6c.

The batch size had considerable effect on the crystallinity index as seen in Table 4. The value of crystallinity index and apparent crystallite size of SFD-CNC2.0 increased with increasing batch size from 100 ml in SFD-CNC2.0 (83.9%, 4.3 nm) up to 500 ml in SFD-CNC2.0-500 (86.9%, 4.3 nm). Similar to highly concentrated suspensions, the batch sizes increased the chances of cellulose nanofibrils ordering through hydrogen bonding and thus resulted in higher crystallinity indices.

Conclusions

CNC agglomerates obtained using spray drying exhibit small impermeable, hard skin packed structure, while those obtained using freeze drying or spray freeze drying exhibit porous interconnected web-like structure. Spray freeze drying of CNC, starting from highly concentrated suspensions (i.e. ∼ 10%) resulted in relatively smaller particles compared to less-concentrated suspensions (0.5–5%). Batch size of CNC suspension had no significant effect on the final properties of the powders. The properties of granulates are influenced by the suspension viscosity (the solid content), geometric parameters of the atomizing nozzle and spraying parameters. Thus, for CNC suspensions having different concentrations, different textures were observed. This was clearly observed in the SEM images, which exhibited various textures with various porous structures depending on the concentration of the suspension (the other parameters being constant).

Spray freeze dried CNC particles resulted in an increase in porosity of ∼ 113 times and ∼ 34 times for freeze dried CNCs compared to spray dried CNC. S_{BET} was inversely proportional to concentration for SFD-CNC, which can be attributed to the reduction in the fibrilous structure and to the partial filling of the pore volume. The preparation of SFD-CNC from different batch sizes resulted in similar BET surface areas suggesting the ease of scale-up to meet industrial demands.

SD-CNC exhibited the highest crystallinity compared to other drying methods, which can be attributed to the heat treatment of the CNCs during the spray drying process and the recrystallization of amorphous cellulose. The crystallinity index of SFD-CNC was affected proportionally with concentration and batch size.

In comparison to conventionally spray dried granulates, spray freeze granulates are much weaker, because capillary forces can be excluded in this technique. The particle size, particle shape (morphology), surface texture (pore size, pore shape, pore size distribution and connectivity), total porosity and surface area of spray freeze dried CNC can be optimized by changing the process parameters including concentration, nozzle size and flow rate in addition to many other factors not examined in this work. These parameters should be examined in details in order to achieve agglomerates (i.e. CNC) with different properties. The ability to control these critical parameters of CNC aggregates makes SFD-CNC more favorable for various applications.

References

Agarwal UP, Ralph SA, Baez C, Reiner RS, Verrill SP (2017) Effect of sample moisture content on XRD-estimated cellulose crystallinity index and crystallite size. Cellulose 24:1971–1984. https://doi.org/10.1007/s10570-017-1259-0

Ahmadzadeh S, Nasirpour A, Keramat J, Hamdami N, Behzad T, Desobry S (2015) Nanoporous cellulose nanocomposite foams as high insulated food packaging materials. Colloids Surf A 468:201–210. https://doi.org/10.1016/j.colsurfa.2014.12.037

Beck S, Bouchard J, Berry R (2012) Dispersibility in water of dried nanocrystalline cellulose. Biomacromolecules 13:1486–1494. https://doi.org/10.1021/bm300191k

Brunauer S, Emmett PH, Teller E (1938) Adsorption of gases in multimolecular layers. J Am Chem Soc 60:309–319

Cao Y, Tan H (2005) Study on crystal structures of enzyme-hydrolyzed cellulosic materials by X-ray diffraction. Enzyme Microb Technol 36:314–317

French AD, Santiago Cintrón M (2013) Cellulose polymorphy, crystallite size, and the Segal Crystallinity Index. Cellulose 20:583–588. https://doi.org/10.1007/s10570-012-9833-y

Habibi Y, Lucia LA, Rojas OJ (2010) Cellulose nanocrystals: chemistry, self-assembly, and applications. Chem Rev 110:3479–3500. https://doi.org/10.1021/cr900339w

Hatakeyama H, Hatakeyama T (1981) Structural change of amorphous cellulose by water- and heat-treatment Die. Makromol Chem 182:1655–1668. https://doi.org/10.1002/macp.1981.021820606

Hindmarsh JP, Russell AB, Chen XD (2003) Experimental and numerical analysis of the temperature transition of a suspended freezing water droplet. Int J Heat Mass Transf 46:1199–1213. https://doi.org/10.1016/S0017-9310(02)00399-X

Hu J, Johnston KP, Williams RO (2003) Spray freezing into liquid (SFL) particle engineering technology to enhance dissolution of poorly water soluble drugs: organic solvent versus organic/aqueous co-solvent systems. Eur J Pharm Sci 20:295–303. https://doi.org/10.1016/s0928-0987(03)00203-3

Ishwarya SP, Anandharamakrishnan C, Stapley AGF (2015) Spray-freeze-drying: a novel process for the drying of foods and bioproducts. Trends Food Sci Technol 41:161–181. https://doi.org/10.1016/j.tifs.2014.10.008

Iyer KA, Schueneman GT, Torkelson JM (2015) Cellulose nanocrystal/polyolefin biocomposites prepared by solid-state shear pulverization: superior dispersion leading to synergistic property enhancements. Polymer 56:464–475. https://doi.org/10.1016/j.polymer.2014.11.017

Jorfi M, Foster EJ (2015) Recent advances in nanocellulose for biomedical applications. J Appl Polym Sci. https://doi.org/10.1002/app.41719

Kamal MR, Khoshkava V (2015) Effect of cellulose nanocrystals (CNC) on rheological and mechanical properties and crystallization behavior of PLA/CNC nanocomposites. Carbohydr Polym 123:105–114. https://doi.org/10.1016/j.carbpol.2015.01.012

Kamal M, Khoshkava V (2017) Spray freeze-dried nanoparticles and method of use thereof. Google Patents

Khoshkava V, Kamal MR (2013) Effect of surface energy on dispersion and mechanical properties of polymer/nanocrystalline cellulose nanocomposites. Biomacromolecules 14:3155–3163. https://doi.org/10.1021/bm400784j

Khoshkava V, Kamal MR (2014) Effect of cellulose nanocrystals (CNC) particle morphology on dispersion and rheological and mechanical properties of polypropylene/CNC nanocomposites. ACS Appl Mater Interface 6:8146–8157. https://doi.org/10.1021/am500577e

Li W, Wang R, Liu S (2011) Nanocrystalline cellulose prepared from softwood kraft pulp via ultrasonic-assisted acid hydrolysis. Bioresources 6:4271–4281

Li M-C, Wu Q, Song K, Lee S, Qing Y, Wu Y (2015) Cellulose nanoparticles: structure–morphology–rheology relationships. ACS Sustain Chem Eng 3:821–832. https://doi.org/10.1021/acssuschemeng.5b00144

Liapis A, Bruttini R (2009) A mathematical model for the spray freeze drying process: the drying of frozen particles in trays and in vials on trays. Int J Heat Mass Transf 52:100–111

Lin N, Dufresne A (2014) Nanocellulose in biomedicine: current status and future prospect. Eur Polym J 59:302–325. https://doi.org/10.1016/j.eurpolymj.2014.07.025

Lin N, Huang J, Dufresne A (2012) Preparation, properties and applications of polysaccharide nanocrystals in advanced functional nanomaterials: a review. Nanoscale 4:3274–3294. https://doi.org/10.1039/c2nr30260h

Liu Y, Zhao Y, Feng X (2008) Exergy analysis for a freeze-drying process. Appl Therm Eng 28:675–690

Lu P, Hsieh Y-L (2010) Preparation and properties of cellulose nanocrystals: rods, spheres, and network. Carbohydr Polym 82:329–336. https://doi.org/10.1016/j.carbpol.2010.04.073

Mariano M, El Kissi N, Dufresne A (2014) Cellulose nanocrystals and related nanocomposites: review of some properties and challenges. J Polym Sci Polym Phys 52:791–806. https://doi.org/10.1002/polb.23490

Meryman HT (1957) Physical limitations of the rapid freezing method. Proc R Soc Lond B Biol Sci 147:452–459

Mihindukulasuriya SDF, Lim LT (2014) Nanotechnology development in food packaging: a review. Trends Food Sci Technol 40:149–167. https://doi.org/10.1016/j.tifs.2014.09.009

Moon RJ, Martini A, Nairn J, Simonsen J, Youngblood J (2011) Cellulose nanomaterials review: structure, properties and nanocomposites. Chem Soc Rev 40:3941–3994. https://doi.org/10.1039/c0cs00108b

Moritz T, Nagy A (2002) Preparation of super soft granules from nanosized ceramic powders by spray freezing. J Nanopart Res 4:439–448. https://doi.org/10.1023/a:1021650415563

Nishiyama Y, Langan P, Chanzy H (2002) Crystal structure and hydrogen-bonding system in cellulose Ibeta from synchrotron X-ray and neutron fiber diffraction. J Am Chem Soc 124:9074–9082. https://doi.org/10.1021/ja0257319

Nyberg B, Carlstrom E, Carlsson R (1991) Granulation of ceramic powders for pressing by spray-freezing and freeze-drying. Euro-Ceramics II 1:447–451

Park S, Baker J, Himmel M, Parilla P, Johnson D (2010) Cellulose crystallinity index: measurement techniques and their impact on interpreting cellulase performance. Biotechnol Biofuels 3:10

Peng YC, Gardner DJ, Han YS (2012) Drying cellulose nanofibrils: in search of a suitable method. Cellulose 19:91–102. https://doi.org/10.1007/s10570-011-9630-z

Peng Y, Gardner DJ, Han Y, Kiziltas A, Cai Z, Tshabalala MA (2013) Influence of drying method on the material properties of nanocellulose I: thermostability and crystallinity. Cellulose 20:2379–2392

Plackett DV, Letchford K, Jackson JK, Burt HM (2014) A review of nanocellulose as a novel vehicle for drug delivery. Nord Pulp Pap Res J 29:105–118

Rajisha KR, Maria HJ, Pothan LA, Ahmad Z, Thomas S (2014) Preparation and characterization of potato starch nanocrystal reinforced natural rubber nanocomposites. Int J Biol Macromol 67:147–153. https://doi.org/10.1016/j.ijbiomac.2014.03.013

Rogers TL, Hu J, Yu Z, Johnston KP, Williams RO (2002) A novel particle engineering technology: spray-freezing into liquid. Int J Pharm 242:93–100. https://doi.org/10.1016/s0378-5173(02)00154-0

Rouquerol J et al (1994) Recommendations for the characterization of porous solids (Technical Report). Pure Appl Chem 66:1739–1758

Rouquerol F, Rouquerol J, Sing KSW (1999) Adsorption by powders and porous solids principles, methodology, and applications. Academic Press. http://worldcat.org; http://site.ebrary.com/id/10190030

Sacui IA et al (2014) Comparison of the properties of cellulose nanocrystals and cellulose nanofibrils isolated from bacteria, tunicate, and wood processed using acid, enzymatic, mechanical, and oxidative methods. ACS Appl Mater Interface 6:6127–6138. https://doi.org/10.1021/am500359f

Segal L, Creely JJ, Martin AE, Conrad CM (2016) An empirical method for estimating the degree of crystallinity of native cellulose using the X-ray diffractometer. Text Res J 29:786–794. https://doi.org/10.1177/004051755902901003

Sing KS (1985) Reporting physisorption data for gas/solid systems with special reference to the determination of surface area and porosity (Recommendations 1984). Pure Appl Chem 57:603–619

Siqueira G, Bras J, Dufresne A (2010) Cellulosic bio-nanocomposites: a review of preparation. Prop Appl Polym Basel 2:728–765. https://doi.org/10.3390/polym2040728

Uhlig M et al (2016) Two-dimensional aggregation and semidilute ordering in cellulose nanocrystals. Langmuir 32:442–450. https://doi.org/10.1021/acs.langmuir.5b04008

Vicent M, Sánchez E, Molina T, Nieto MI, Moreno R (2012) Comparison of freeze drying and spray drying to obtain porous nanostructured granules from nanosized suspensions. J Eur Ceram Soc 32:1019–1028. https://doi.org/10.1016/j.jeurceramsoc.2011.11.034

Wang Y, Kho K, Cheow WS, Hadinoto K (2012) A comparison between spray drying and spray freeze drying for dry powder inhaler formulation of drug-loaded lipid–polymer hybrid nanoparticles. Int J Pharm 424:98–106

Wanning S, Suverkrup R, Lamprecht A (2015) Pharmaceutical spray freeze drying. Int J Pharm 488:136–153. https://doi.org/10.1016/j.ijpharm.2015.04.053

Yildiz S, Gümüşkaya E (2007) The effects of thermal modification on crystalline structure of cellulose in soft and hardwood. Build Environ 42:62–67. https://doi.org/10.1016/j.buildenv.2005.07.009

Yoshida H, Saeki T, Hashimoto K, Fujioka T (1991) Size classification of submicron powder by air cyclone and three-dimensional analysis. J Chem Eng Jpn 24:640–647. https://doi.org/10.1252/jcej.24.640

Zhang W, He X, Li C, Zhang X, Lu C, Zhang X, Deng Y (2013) High performance poly (vinyl alcohol)/cellulose nanocrystals nanocomposites manufactured by injection molding. Cellulose 21:485–494. https://doi.org/10.1007/s10570-013-0141-y